Crystal Structure and Morphology of Mixed $Cr_{1-x}Al_xN$ Nitride Precipitates: Gaseous Nitriding of a Fe-1.5 Wt Pct Cr-1.5 Wt Pct Al Alloy

A.R. CLAUSS, E. BISCHOFF, S.S. HOSMANI, R.E. SCHACHERL, and E.J. MITTEMEIJER

The crystal structure and morphology of nitride precipitates developing in the matrix of a Fe-1.5 wt pct Cr-1.5 wt pct Al (Fe-1.6 at. pct Cr-3.1 at. pct Al) alloy upon gas nitriding were investigated. To this end, the nitrided zone was studied using metallographic methods, X-ray diffractometry (XRD), electron probe microanalysis (EPMA), microhardness measurement, and transmission electron microscopy (TEM), including high-resolution TEM (HRTEM), and scanning TEM (STEM). Furthermore, a nitrogen-absorption isotherm was determined, for use in characterizing the nature of the nitride-precipitation process. It could be shown that the expected equilibrium nitrides, cubic CrN and hexagonal AlN, do not develop. Instead, mixed $Cr_{1-x}Al_xN$ nitride precipitates of the cubic, rock-salt structure type develop upon nitriding the ternary alloy. These precipitates obey a Bain-type orientation relationship (OR) with the ferrite matrix and are associated with a considerable uptake of excess nitrogen and a very pronounced hardness increase.

DOI: 10.1007/s11661-009-9865-6

I. INTRODUCTION

NITRIDING is an important thermochemical surface engineering process of ferritic steel workpieces for improving the resistance against fatigue, wear, and corrosion.[1–4] Although this treatment is widely used in industry, the application practice is largely based on phenomenology. The presence of alloying elements such as Al, Cr, Ti, and V, which have a strong affinity for nitrogen, can lead to the formation of nitride precipitates in the ferrite matrix, which, by mechanical strengthening, are to a large extent responsible for the resulting strongly improved mechanical performance.

Until now, nitride precipitates in ferrite matrices have only been investigated in detail for simple binary iron-based alloys (*e.g.*, References 5 through 8). In practice, however, more than one alloying element with an affinity for nitrogen occurs in technical alloys. In particular, Al and Cr are used together as alloying elements in typical nitriding steels. Hence, a strong technological interest stimulates the investigation of the composition, structure, and shape of nitride precipitates in such multicomponent alloys. At the same time, there also exists a pronounced fundamental, scientific importance for such research. Upon the nitriding of these alloys, one would expect the precipitation of the equilibrium nitrides cubic CrN and hexagonal AlN. However, this does not occur, as shown in this article. Instead, metastable mixed nitrides develop and these are responsible for the resulting favorable technological properties.

A. *Nitrides in Binary Ferritic Alloys*

A significant amount of research on the nitriding of binary iron-based alloys has been done both in the past and in recent years. The formation of plateletlike nitride precipitates obeying the Bain-type orientation relationship (OR)[9] (sometimes also named for Baker and Nutting[10]) during the nitriding of binary low-alloyed ferritic irons has been observed for pure Fe-Cr, Fe-V, Fe-Ti, and Fe-Mo alloys.[7,11–13] The nitride-precipitation kinetics during (gaseous) nitriding has been classified according to the type of alloying element-nitrogen interaction (weak, intermediate, or strong).[14]

The nitriding of binary Fe-Cr[6,11,15–21] and Fe-Al[5,22–28] alloys has been investigated rather extensively. Three modifications of chromium nitride can be distinguished, as follows: (1) the cubic, rock-salt structure type CrN, (2) the hexagonal structure type Cr_2N, and (3) an orthorhombic CrN modification, which occurs only at very low temperatures (cryogenic modification) and is not relevant for the nitriding of iron-based alloys.[29] For aluminum nitride, three modifications also exist, as follows: (1) the at-ambient pressure thermodynamically stable hexagonal wurtzite structure type AlN,[29,30]

A.R. CLAUSS, Ph.D., previously with the Max Planck Institute for Metals Research, is with Robert Bosch GmbH, Stuttgart 70049, Germany. E . BISCHOFF, Dr. rer. nat., is with the Max Planck Institute for Metals Research, Stuttgart 70569, Germany. S.S. HOSMANI, Scientist, formerly with the Max Planck Institute for Metals Research, is with Case Western Reserve University, Cleveland, OH 216-368-2000. R.E. SCHACHERL, Scientist, is with the Institute for Materials Science, University of Stuttgart, Stuttgart 70569, Germany. Contact e-mail: r.schacherl@mf.mpg.de E.J. MITTEMEIJER, Director, Max Planck Institute for Metals Research, is Professor, Institute for Materials Science at the University of Stuttgart.
Manuscript submitted September 18, 2008.
Article published online June 20, 2009

(2) the metastable cubic, rock-salt structure type AlN,[5] and (3) the metastable zinc blende structure type AlN,[31,32] which has never been observed in nitrided iron-based alloys. In ferritic Fe-Cr alloys, the formation of cubic, rock-salt structure type CrN platelets with a Bain-type OR with the ferrite matrix was observed.[11,33] In annealed Fe-Al alloys, the nucleation of the thermodynamically stable hexagonal wurtzite structure type AlN is difficult.[23,25,26,34] The transmission electron microscopy (TEM) results of Biglari *et al.*[5] from a Fe-2 at. pct Al alloy revealed the presence of two AlN modifications after long-time nitriding: (1) the hexagonal wurtzite structure type AlN exhibiting a Pitsch–Schrader[35] OR with the ferrite matrix and (2) the cubic, rock-salt structure type AlN showing a Bain OR with the ferrite matrix.

Upon the nitriding of ferritic iron-based alloys, more nitrogen is taken up than is necessary for the formation of nitride precipitates and for the dissolution of nitrogen in a pure unstrained ferrite matrix. This additional nitrogen present in the nitrided zone is called "excess nitrogen."[36]

B. *Nitrides in Ternary Ferritic Alloys*

There is sparse and ambiguous information about the nitriding behavior of iron-based alloys containing both Cr and Al as alloying elements; work on the nitriding of the ternary system Fe-Cr-Al is totally lacking. In a nitrided Cr-Al medium-carbon steel, "distorted" platelets approximately parallel to $\{001\}_{\alpha\text{-Fe}}$ matrix planes were observed.[37] After the nitriding of low-carbon Al- and Cr-containing steels, in addition to iron nitrides and hexagonal AlN, the formation of an fcc Me_xN nitride ($x \approx 1$) with Me-containing Al and, presumably, Cr was reported.[38] An investigation of nitrided (Cr, Al, Ni)- and (Cr, Al, Mn)-containing nitriding steels suggested the formation of tiny coherent plateletlike mixed (*i.e.*, Cr- and Al-containing) nitrides with a distinct OR (*i.e.*, Bain) to the ferrite matrix,[39–41] but evidence for the simultaneous occurrence of Cr and Al in the nitride precipitates was not provided.

The present article describes the nitriding behavior of a recrystallized ternary Fe-Cr-Al alloy: Fe-1.5 wt pct Cr-1.5 wt pct Al. The gaseous* nitriding conditions were chosen such that no iron nitrides develop at the surface: Upon nitriding (only), precipitation of the alloying element nitrides in the ferritic matrix takes place. The results obtained show that the nitriding behavior of this ternary Fe-Cr-Al alloy is not given by a simple "addition" of the nitriding behaviors of the bounding binary Fe-Cr and Fe-Al systems. The nitrided samples were investigated with respect to the microstructure, phase constitution, and element distribution using X-ray diffractometry (XRD), electron probe microanalysis (EPMA), light microscopy (LM), microhardness measurement (Vickers), high-resolution TEM (HRTEM), and scanning TEM (STEM). According to the knowledge of the present authors, this is the first time that, on the basis of the gaseous nitriding of a Fe-Cr-Al alloy, the occurrence of tiny platelets of a cubic, rock-salt structure type, mixed $Cr_{1-x}Al_xN$ nitride precipitates obeying the Bain-type OR with the ferrite matrix is proven directly by nanoscale analytical methods.

*The gaseous nitriding variant enables an accurate adjustment of the thermodynamic condition (chemical potential of nitrogen dissolved in the solid) at the sample surface.[4]

II. EXPERIMENTAL

A. *Specimen Preparation and Nitriding*

Samples with the composition of Fe-1.5 wt pct Cr-1.5 wt pct Al (Table I) and a rectangular shape with the dimensions of $20 \times 15 \times 1$ mm^3 were produced (Reference 8). The nitriding process was performed in a H_2/NH_3 gas mixture (purity H_2: 99.999 vol pct, purity NH_3: >99.998 vol pct) at a temperature of (853 ± 1) K and at a nitriding potential[42] $r_N = 0.104$ atm$^{-1/2}$ (Reference 8).

Before nitriding, the recrystallized specimen surfaces were polished mechanically (the last step was a 1-μm diamond suspension), cleaned (first with ethanol and, finally, with water in an ultrasonic bath), and thereafter dried in a nitrogen gas flow.

B. *Specimen Characterization*

The specimen characterization was performed by applying XRD, EPMA, LM, and microhardness measurements (Reference 6).

1. *Transmission electron microscopy*

The TEM specimens taken at selected depths of the nitrided zone were produced by argon ion milling in a manner similar to that described in References 43 and 46.

The TEM investigation was performed using a PHILIPS** CM 200 transmission electron microscope operating at 200 kV, equipped with an energy-dispersive

**PHILIPS is a trademark of Philips Electronic Instruments Corp., Mahwah, NJ.

Table I. Amounts of Alloying Elements and Impurities of Used Alloy (Balance Fe)

	CR		Al					
Alloy	(Wt Pct)	(At. Pct)	(Wt Pct)	(At. Pct)	N (Wt Pct)	O (Wt Pct)	S (Wt Pct)	C (Wt Pct)
Fe-Cr-Al	1.52 ± 0.01	1.60 ± 0.01	1.52 ± 0.01	3.09 ± 0.02	<0.0005	0.0043 ± 0.0004	<0.0010	0.0025 ± 0.0002

X-ray (EDX) detection system. Bright-field (BF) and dark-field (DF) images and selected-area diffraction patterns (SADPs) were taken by a charge-coupled device camera. The lattice spacings d were calculated for different $\{hkl\}$ values and phases from the lattice parameters a, as provided by the International Centre for Diffraction Data (Newtown Square, PA) database[44] (α-Fe: $a = 0.287$ nm, Fe_3O_4: $a = 0.839$ nm, AlN wurtzite: $a = 0.311$ nm, AlN rock salt: $a = 0.405$ nm, AlN zinc blende: $a = 0.434$ nm, and CrN rock salt: $a = 0.414$ nm). The d values of AlN and CrN rock-salt structures are so close to each other that it is very difficult to distinguish these phases in TEM diffraction patterns. The corresponding d values of the diffraction spots were determined[47] by measuring the distance R from the center in the SADP with the Digital Micrograph Diffpack program (Gatan, Inc., Pleasanton, CA) Calibration was achieved either by calculation from the acceleration voltage U_B or the camera length L or by internal calibration, using ferrite matrix spots of which the d values are known. The latter method was applied in most cases. These measured d values of the diffraction spots were compared with the calculated d values mentioned earlier to index the diffraction spots and identify the present phases.

2. *STEM and HRTEM*

The STEM investigation was performed using a VG HB 501UX scanning transmission electron microscope (VG Microscopes Ltd., East Grinstead, UK) operating at 100 kV with a focused beam less than 1 nm in size and equipped with a NORAN energy-dispersive X-ray (EDX) spectroscopy system (Thermo Fisher Scientific Inc., Waltham, MA) with a multichannel analyzer (10 eV per channel) for chemical analysis. For each line scan across a nitride precipitate. 30 points was measured with a dwell time of 5 seconds per point (evaluation software: NORAN System SIX).

The HRTEM was performed using a JEOL[†] high-voltage atomic-resolution microscope operating at 1250 kV.

[†]JEOL is a trademark of Japan Electron Optics Ltd., Tokyo.

C. *Determination of Nitrogen-Absorption Isotherm*

For a quantitative analysis of the excess nitrogen uptake, a nitrogen-absorption isotherm was determined (Reference 48 for background on the measurement of the nitrogen absorption). For this purpose, rectangular foils ($20 \times 15 \times 0.2$ mm^3) were prepared. Prenitriding was performed at (853 ± 1) K for 24 hours in a H_2/NH_3 gas mixture corresponding to a nitriding potential of $r_N = 0.104$ atm$^{-1/2}$ (Section A). After the prenitriding, the (then constant amount of) nitrogen is distributed homogeneously over the whole cross section, as proven by EPMA. Subsequently, the prenitrided foil was denitrided at a (lower) temperature of (743 ± 1) K for 48 hours in a pure hydrogen gas flow (500 mL/min), to remove nitrogen that is not strongly bonded (to the alloying elements) without changing the microstructure.

The data for the nitrogen-absorption isotherm were then determined by nitriding the foil at (833 ± 1) K for 30 hours, applying four different nitriding potentials: $r_N = 0.054$, 0.091, 0.117, and 0.140 atm$^{-1/2}$. After each nitriding step, a denitriding (as before) step was performed. The change in the nitrogen content after each nitriding and denitriding was measured by weighing the foil on a Mettler microbalance (Mettler-Toledo Inc., Columbus, OH) with an accuracy of 1 μg. For each nitriding/denitriding state, 20 weightings were carried out to determine an average mass value. The resulting errors in the mass differences upon nitriding/denitriding are smaller than the size of the data points in the absorption isotherm (Section III–D).

III. RESULTS AND EVALUATION

A. *Phase Analysis*

The X-ray diffraction analyses were carried out on the specimen surface before and after nitriding. After nitriding, no new phases are detectable in the diffractograms recorded from the specimen surface (Figure 1), but the peaks of the ferrite matrix had very strongly broadened.

B. *Composition and Microhardness Depth Profiles*

The EPMA concentration depth profiles of N and the two nitride-forming elements Al and Cr are shown in Figure 2(b) (the results of five single line scans, taken from different sites on the cross section perpendicular to the surface, are shown together, superimposed graphically in one concentration depth profile).[‡] Except at the surface, where the atomic concentration of Al and Cr is

[‡]The specimen becomes very brittle and develops cracks upon nitriding. This is discussed in Ref. 66.

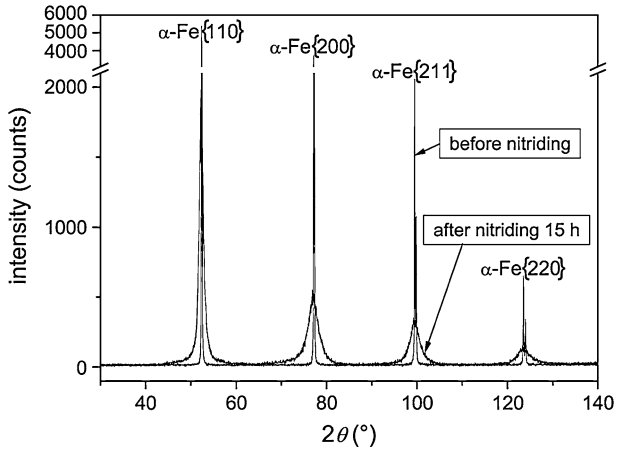

Fig. 1—X-ray diffractograms recorded from the surface of the specimen before and after nitriding (15 h at 853 K): A considerable peak broadening of the ferrite peaks is observed after nitriding.

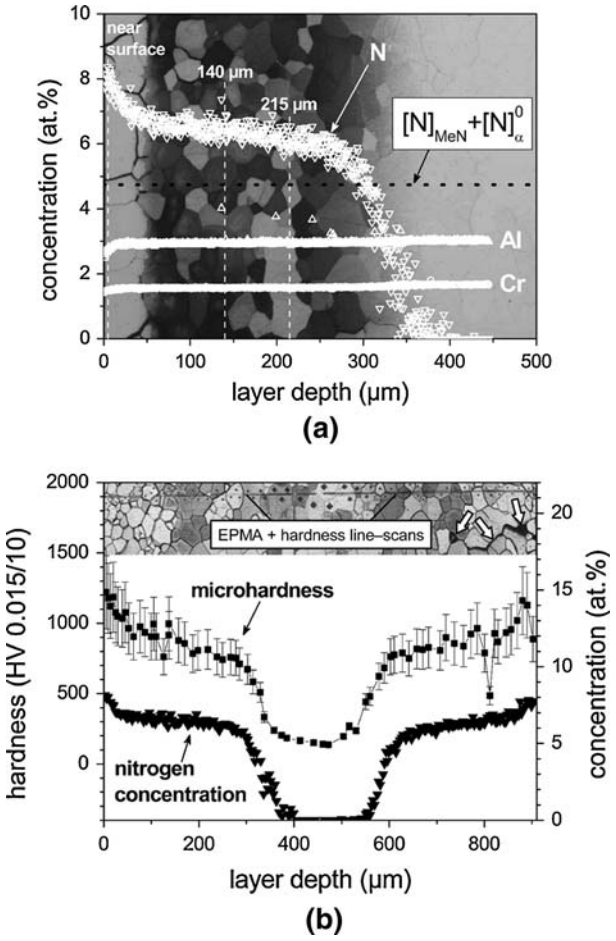

Fig. 2—(*a*) N, Al, and Cr (EPMA) concentration depth profiles of a nitrided specimen (15 h at 853 K) combined with corresponding LM micrograph. Dashed vertical white lines denote depth values from which TEM samples were prepared. Dotted horizontal black line denotes amount of N necessary to transform all alloying elements into alloying element nitrides plus amount of nitrogen dissolved interstitially in unstrained remaining ferrite matrix. (*b*) Microhardness and N-concentration depth profiles after nitriding; the corresponding LM micrograph is also shown in (b).

slightly decreased as a consequence of a distinct near-surface increase in the N concentration, the Al and Cr concentrations are approximately constant over the cross section. At some sites in the EPMA line scans, the electron beam hits single pores. These pores cause a seeming increase in the concentrations of light elements such as Al and N, because the physical assumptions used in the quantitative evaluation of the element concentrations (absorption and atomic number correction) are not fulfilled near pores.[45] The N-concentration depth profile (Figure 2(b)) is characterized by the following: (1) a strong decrease in the N content toward a larger depth near the surface, (2) a subsequent plateau region of N content with a modest negative slope, and (3) the transition zone between the nitrided layer and the unnitrided core, where the N concentration drops to zero.

Immediately after EPMA, the embedded cross section was etched, to uncover the line scans of the electron beam (revealed by the carbon deposition, (the LM micrograph shown in Figure 2(c)). Along two (of the five) EPMA line scans (one started from the left surface and the other started from the opposite, right surface of the specimen cross section) (the LM micrograph in Figure 2(c)), the microhardness values were determined. The obtained N-concentration depth profile can be compared with the corresponding microhardness depth profile in Figure 2(c). The microhardness distribution over the cross section shows the same characteristics as the N-concentration depth profile. The pronounced increase in hardness contributes distinctly to the improved mechanical performance by nitriding.[1,2]

The dotted horizontal line in Figure 2(b) denotes the so-called normal amount of N, ($[N]_{normal} = 4.74$ at. pct) necessary to transform all substitutionally dissolved Al and Cr into nitride precipitates (*i.e.*, $[N]_{MeN}$) plus the amount of N that can be dissolved interstitially in the remaining pure, unstrained ferrite matrix in the thermodynamic equilibrium at the applied nitriding conditions (*i.e.*, $[N]^0_{\alpha\text{-Fe}}$). The value $[N]^0_{\alpha\text{-Fe}} = 0.30$ at. pct was experimentally determined under conditions similar to those applied to the nitriding of the ternary Fe-Cr-Al alloy, by nitriding a pure ferrite foil.[48] The amount of N in excess of this normal amount of N is called excess nitrogen[15,36,49] (Section D). Evidently (Figure 2(b)), during nitriding, the specimens take up much more N than is necessary for the stoichiometric formation of the nitride precipitates and the realization of the equilibrium N solubility in the ferrite matrix.

C. *TEM Analysis*

The TEM analysis was carried out to identify the precipitated nitride phase(s). The dashed vertical white lines in the cross section shown in Figure 2(b) indicate the depths at which the TEM samples were prepared.

1. *Crystallography of nitride precipitates and deformation structure*

The SADPs (zone axis: $[001]_{\alpha\text{-Fe}}$) of the nitrided surface region (15 hours at 853 K) that correspond to the DF images presented in Figures 3(a) and (b) show, in addition to the bright ferrite matrix spots, streaks with accumulations in intensity. These intensity accumulations are interpreted as nitride diffraction spots; they are compatible with the occurrence of reflections due to nitride precipitates of the rock-salt structure type of both CrN and AlN. The locations of the accumulations indicate that the Bain-type OR[9] holds for the nitride precipitates and the ferrite matrix:

$$\{001\}_{\alpha\text{-Fe}}//\{001\}_{MeN}, \langle 100\rangle_{\alpha\text{-Fe}}//\langle 110\rangle_{MeN}; Me = Cr, Al$$

There are three variants of the Bain OR between the ferrite and cubic, rock-salt structure type precipitates (Table II and Figures 3(c) through (e)). The superposition of these three variants leads to the characteristic SADP shown in Figure 3(f). On the experimental SADPs shown in Figures 3(a) and (b), discrete spots are visible at the locations of the forbidden $\{100\}_{\alpha\text{-Fe}}$ reflections; these are due to $\{220\}_{Fe_3O_4}$ reflections from

Fe_3O_4, which unavoidably developed at the surface of the foil used for the TEM analysis.[5,17,50]

Tiny plateletlike structures are visible in the DF images taken from the rock-salt 002_{MeN} spots of two different variants of the Bain OR (the circles in the SADP) pertaining to nitride precipitates, which are oriented perpendicular to each other (Figures 3(a) and (b)). The length of the precipitate platelets can be estimated from the DF images in Figures 3(a) and (b) and is approximately 10 nm (and smaller).

A DF image obtained using a $\{002\}_{MeN}$ spot of the rock-salt structure type nitride precipitate and the corresponding SADP from a nitrided depth of approximately 140 μm is shown in Figure 4(a). Plateletlike structures that obey the Bain OR are visible. The length of the precipitates (the lateral size of the platelets) at this depth is in the range of approximately 100 nm and, hence, is 10 times larger than is the case near the surface in the same specimen (Figures 3(a) and (b)).

A BF image and the corresponding SADP from a nitrided depth of approximately 215 μm are shown in Figures 4(b). The incident electron beam is not exactly parallel to the $[001]_{\alpha\text{-Fe}}$ zone axis. Platelets oriented more or less perpendicular to each other can be seen in the BF image; the platelets are surrounded by strain-field contrast. The size of the precipitates at this depth of 215 μm is in the same range as that seen at a depth of 140 μm (Figures 4(a) and (b)). Apparently, the precipitate platelets in Figure 4(a) are partly nonplanar (the arrows in Figure 4(a)) and the precipitates are not oriented exactly perpendicular to each other. Further, a variation in the brightness along a platelet in the DF image occurs (Figure 5(a)); this is associated with a spreading (“splitting up”) of the $\{002\}_{MeN}$ diffraction spots (Figure 5(b)). Both observations are compatible with the bending and local distortion of the platelets (refer to Figure 6 and its discussion in Reference 59).

2. *High-resolution transmission electron microscopy*

An HRTEM image (zone axis: $[001]_{\alpha\text{-Fe}}$) of an ion-milled TEM specimen taken near the nitrided surface and a fast Fourier transformation (FFT) pattern from a selected region of the image (white square) are shown in Figure 6(a). In the white-squared area, two tiny platelet-like precipitates are visible that are oriented perpendicular to each other (arrows). The FFT pattern is congruent with variants 2 and 3 of the Bain OR (Table II and Figures 3(d) and (e)), including the oxide spots.

The inverse FFT image of the ferrite matrix, which contains a tiny precipitate (with a thickness of

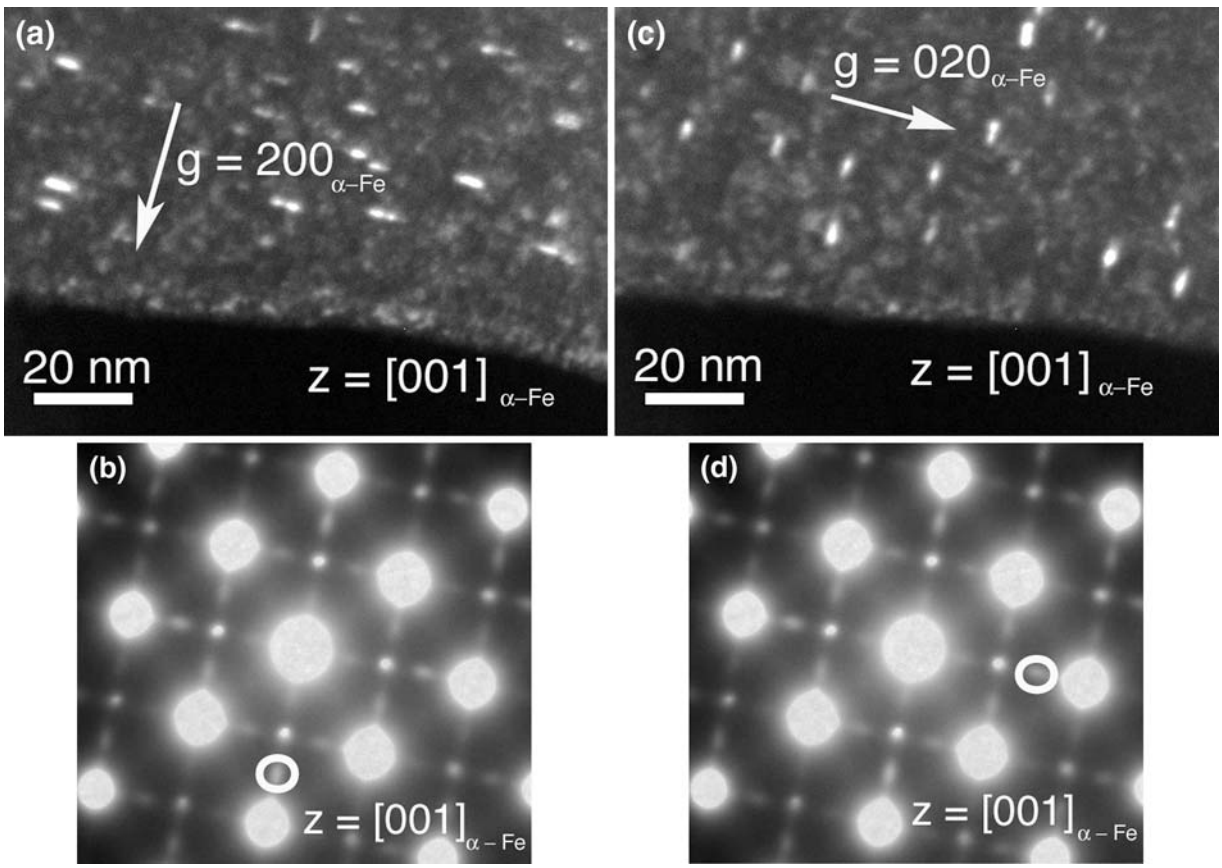

Fig. 3—(*a*) and (*c*) DF images and (*b*) and (*d*) corresponding SADPs of an ion-milled TEM specimen from near the nitrided surface (a depth of a few microns); the DF images are obtained from $\{002\}_{MeN}$ spots of the rock-salt structure type of the nitride precipitates in a Bain OR with the ferritic matrix ((f) and (g)). (*e*) through (*g*) Schematic SADPs (zone axis: $[001]_{\alpha\text{-Fe}}$) of the three variants 1, 2, and 3 of the Bain OR between the ferritic matrix and cubic, rock-salt structure type nitride precipitates, and their superposition in (*h*). Transparent circles: α-Fe spots; black circles: cubic, rock-salt structure type spots; crossed circles: $\{220\}Fe_3O_4$ spots.

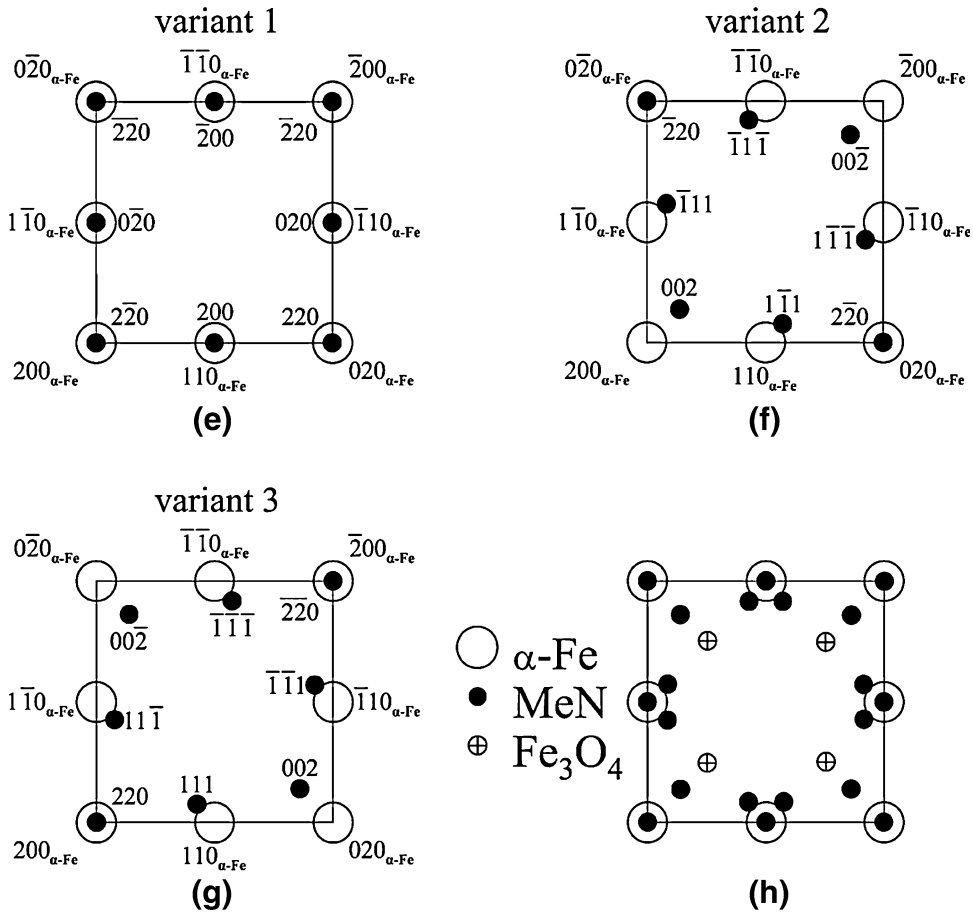

Fig. 3—Continued.

Table II. Three Variants of Bain OR between Ferrite and Cubic, Rock-Salt Structure Type Precipitates (Figures 3(c) through (e))

Bain OR		
Variant 1	Variant 2	Variant 3
[100]α-Fe//$[1\bar{1}0]$MeN	[100]α-Fe//[001]MeN	[100]α-Fe//[110]MeN
[010]α-Fe//[110]MeN	[010]α-Fe//$[1\bar{1}0]$MeN	[010]α-Fe//[001]MeN
[001]α-Fe//[001]MeN	[001]α-Fe//[110]MeN	[001]α-Fe//$[1\bar{1}0]$MeN

approximately 1 nm) obeying the Bain OR (visible in the lower right corner (arrow)) of the white-squared area in Figure 6(a) and which was obtained using the $\{110\}_{\alpha\text{-Fe}}$ and $\{200\}_{\alpha\text{-Fe}}$ ferrite spots and precipitate spots corresponding to variant 2 of the Bain OR (Table II and Figure 3(d)), is shown in Figure 6(b) (the FFT image in the upper right corner of Figure 6(b)). The precipitate is partially coherent with the ferrite matrix. A few dislocations have been observed in the ferrite matrix surrounding a precipitate (Burgers circuit analysis).

3. *Composition of nitride precipitates*

A STEM BF image of a precipitate taken at a nitrided depth of approximately 215 μm is shown in Figure 7(a). Although the quality of the BF images is poor due to an uncorrectable astigmatism caused by the ferromagnetism of the TEM specimens, a plateletlike precipitate that appears bright against its dark surroundings is visible in Figure 7(a). The arrow in the BF image depicts the path of the EDX line scan. The Cliff–Lorimer ratio technique[51] was applied for the quantitative analysis of Fe, Cr, and Al, considering the X-ray absorption and assuming a maximum TEM foil thickness of 200 nm. Due to the drift of the sample, the counting time was limited and reliable results for the N concentration could not be obtained, for which reason N was not taken into account for the quantitative analysis. The results for Cr and Al have been plotted as a concentration in atomic percent *vs* the distance along the depicted path and are shown in Figure 7(b). Evidently, in the

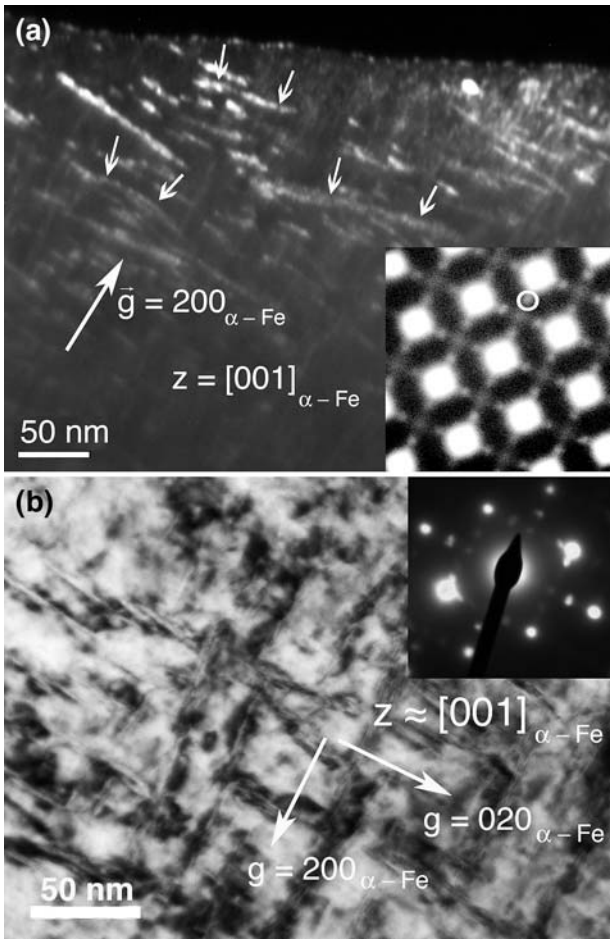

Fig. 4—(*a*) DF image obtained from a 002_{MeN} spot of the rock-salt structure nitride precipitate and corresponding SADP (electron-beam axis: $[001]_{\alpha\text{-Fe}}$) of an ion-milled TEM specimen from a nitrided depth of approximately 140 μm; MeN with Bain OR with the ferrite matrix (Fig. 3: variant 2). (*b*) BF image and corresponding SADP (electron-beam axis near $[001]_{\alpha\text{-Fe}}$) of an ion-milled TEM specimen from a nitrided depth of approximately 215 μm. Note the strain-field contrast around the precipitates.

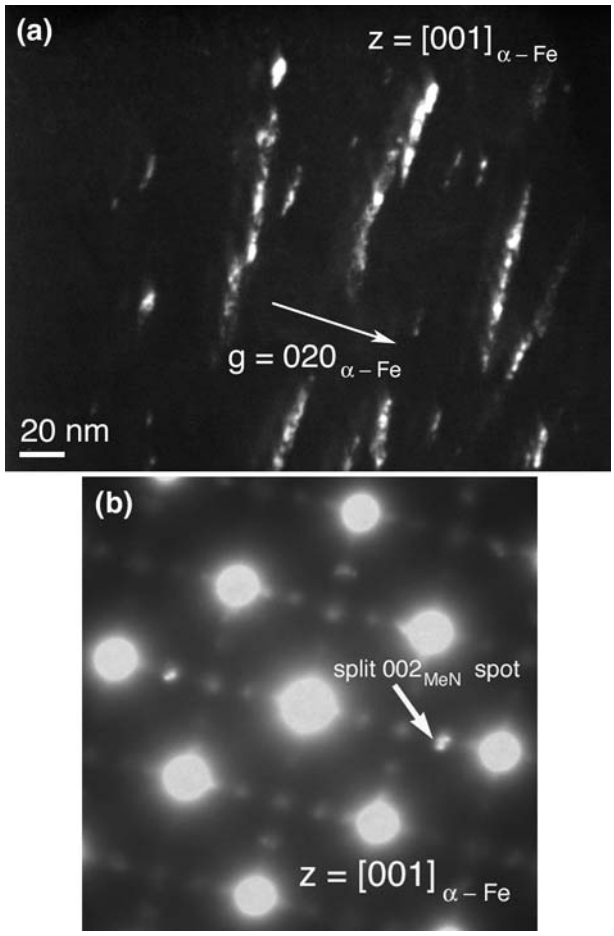

Fig. 5—(*a*) DF image obtained from a 002_{MeN} spot of the rock-salt structure nitride precipitate of an ion-milled TEM specimen from a nitrided depth of approximately 215 μm. Along each platelet, a variation in the brightness occurs. (*b*) Corresponding SADP (electron-beam axis: $[001]_{\alpha\text{-Fe}}$) SADP of Fig. 5(a) showing spreading (splitting up) of the 002_{MeN} spot of the rock-salt structure nitride precipitate with Bain OR with the ferrite matrix.

precipitate, the alloying elements Cr and Al are both present. Although the atomic fractions shown in Figure 7(b) can only be considered relatively (because N was not taken into account, as mentioned earlier), the measurements do indicate that a higher atomic fraction of Al than Cr is contained in the nitride, which is compatible with the composition of the alloy, assuming that all of the Cr and all of the Al have precipitated as mixed nitride.

D. *Analysis of excess nitrogen uptake*

The nitrogen concentration $[N]_{total}$ in the Fe-1.5 wt pct Cr-1.5 wt pct Al foil (*i.e.*, Fe-1.58 at. pct Cr-3.07 at. pct Al) upon mass increase after homogeneous prenitriding (Section II–C) was (5.911 ± 0.004) at. pct. The normal N uptake $[N]_{normal} = [N]_{(Cr,Al)N} + [N]^0_{\alpha\text{-Fe}}$ after prenitriding, where $[N]_{(Cr,Al)N}$ is the amount of N incorporated in the nitride precipitate and $[N]^0_{\alpha\text{-Fe}}$ is the equilibrium solubility of N in the unstrained ferrite matrix that corresponds to the applied temperature and nitriding potential,[§] can be calculated as (4.650 ± 0.004) at. pct, assuming that all the Al and Cr have formed nitride precipitates (either AlN and CrN or (Al, Cr)N). Hence, the total amount of excess nitrogen that follows from $[N]^{excess}_{total} = [N]_{total} - [N]_{normal}$. $[N]^{excess}_{total}$ has the following two parts: (1) mobile excess nitrogen, *i.e.*, extra dissolved N due to the tensile hydrostatic component of misfit stress in the ferrite matrix,[36] $[N]_{strain}$ and (2) immobile excess nitrogen. Immobile excess nitrogen consists of two components: N segregated at dislocations $[N]_{dislocations}$ and N adsorbed at the platelet faces $[N]_{interface}$. Due to the low dislocation density in recrystallized foils, $[N]_{dislocations}$ can be neglected and, thus, $[N]_{strain} + [N]_{interface} = (1.261 \pm 0.004)$ at. pct.

[§]The equilibrium solubility of N in ferrite $[N]^0_{\alpha\text{-Fe}}$ at 853 K for the nitriding potential of $r_N = 0.104\ atm^{-1/2}$ was determined by nitriding a pure ferrite foil:[48] 0.30 at. pct (Section III–B).

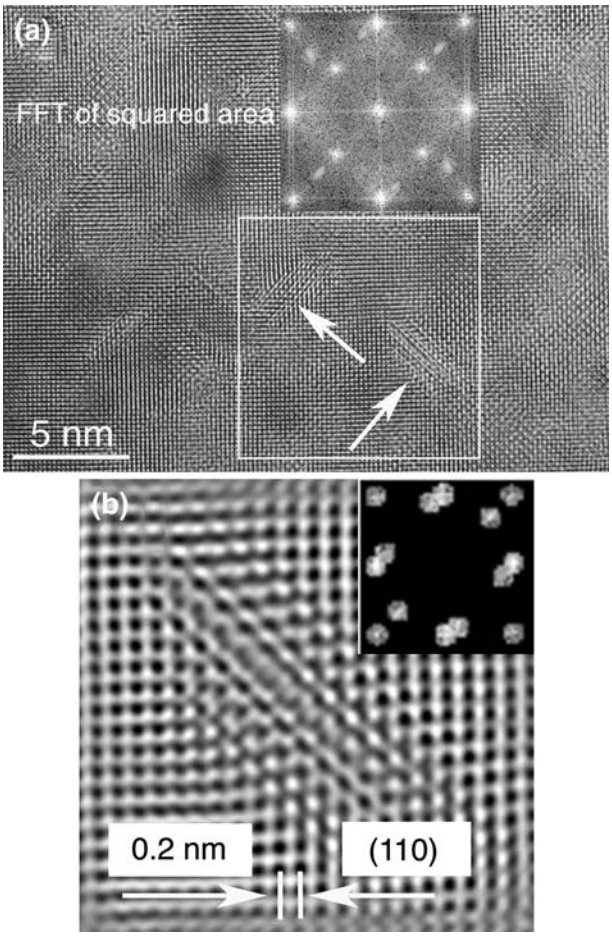

Fig. 6—(*a*) HRTEM image of an ion-milled TEM specimen from near the nitrided surface (electron-beam axis: $[001]_{\alpha\text{-Fe}}$). The FFT pattern was generated from the area within the white square. (*b*) Inverse FFT filtered image of the ferrite matrix with precipitate, using $\{110\}_{\alpha\text{-Fe}}$ and $\{200\}_{\alpha\text{-Fe}}$ spots and precipitate spots corresponding to Bain OR variant 2 (Table II and Fig. 3(d)).

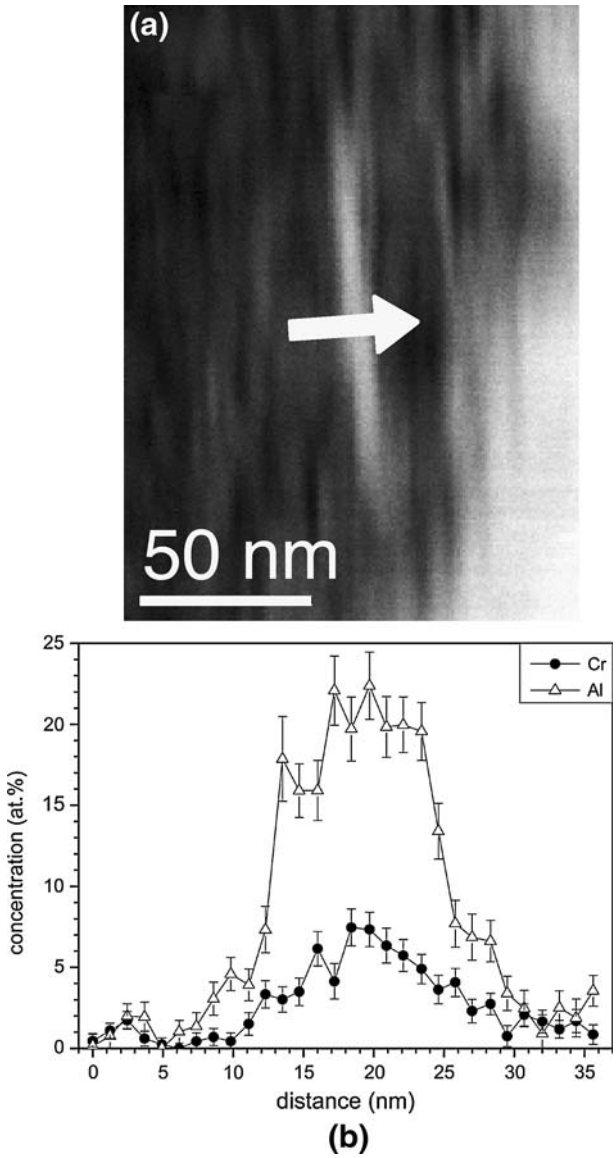

Fig. 7—(*a*) STEM BF image of a precipitate in an ion-milled specimen from a nitrided depth of approximately 215 μm (specimen nitrided for 15 h at 853 K). The image is strongly astigmatic because of the ferromagnetism of the specimen. (*b*) Results of the EDX line scan (indicated by arrow in (a)). Both alloying elements Al and Cr are present in the precipitate. The atomic fraction values can only be applied relatively.

After prenitriding, the foil was denitrided (Section II–C). The remaining amount of N after denitriding, as determined by weight measurement, was (4.527 ± 0.001) at. pct. The amount of N necessary to transform all the Cr and Al into nitride precipitates (*i.e.*, $[N]_{(Cr,Al)N} = [Cr]_{Cr_{1-x}Al_xN} + [Al]_{Cr_{1-x}Al_xN}$) is (4.445 ± 0.001) at. pct and, hence, is only 0.082 at. pct lower than the experimentally remaining N concentration after denitriding. It is concluded that the N remaining after denitriding is the N strongly bonded in and at the MeN precipitates (Section IV–D).

The results of the prenitriding and denitriding experiments are summarized in Figure 8(a), in which the N content is expressed as the number of N atoms taken up per 100 (Fe + Cr + Al) matrix atoms.

In order to identify the contributions of the mobile and immobile excess nitrogen in the total amount of excess nitrogen, a nitrogen-absorption isotherm at 833 K was determined (Figure 8(b) for the Fe-1.5 wt pct Cr-1.5 wt pct Al foil after prenitriding (at 853 K) and denitriding (at 743 K)). The N level after denitriding that was mentioned earlier has been indicated by "A." The expected amount of N required for the formation of the $Cr_{1-x}Al_xN$ precipitates (*i.e.*, $[N]_{(Cr,Al)N}$) has been indicated by "C." At a constant temperature, the amount of interstitially dissolved N in the ferrite matrix increases linearly with r_N.[4,42] Thus, the straight line dependence above level "B" in Figure 8(b) represents the N dissolved interstitially in the ferrite matrix. Fitting a straight line to all four square data points leads to the dashed line in Figure 8(b), which intersects the ordinate at $r_N = 0$; the point of intersection has been indicated by B.

The difference between levels B and C corresponds to the N taken up in excess of the amount needed to form the $Cr_{1-x}Al_xN$ precipitates. In accordance with the

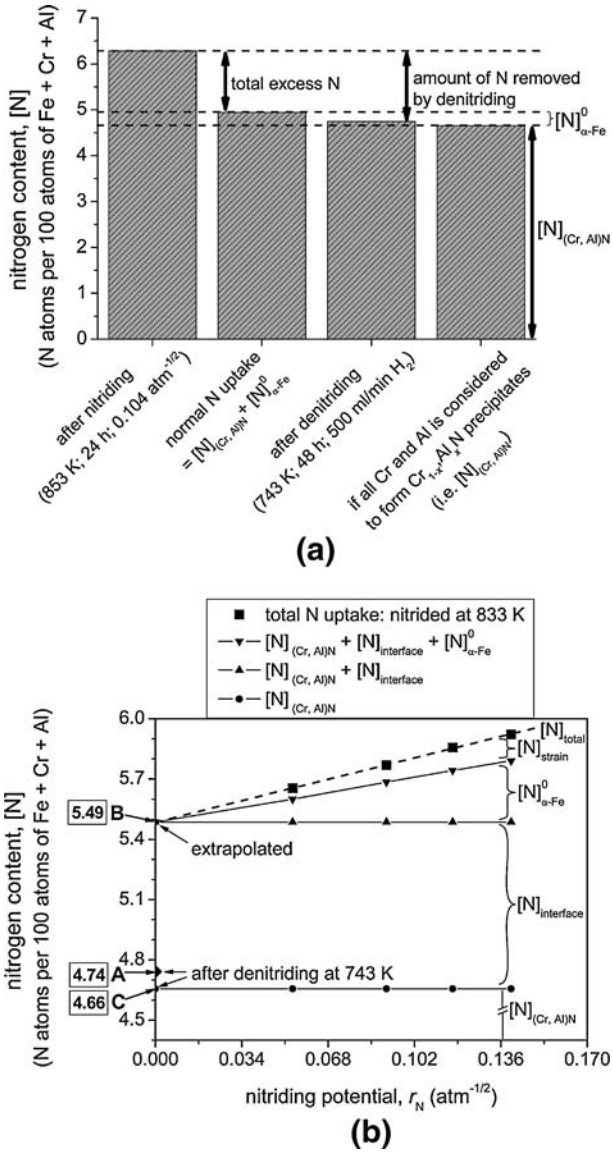

Fig. 8—(*a*) Summary of the prenitriding (24 h at 853 K, $r_N = 0.104$ atm$^{-1/2}$) and denitriding (48 h at 743 K in pure H_2) experiments performed with a Fe-1.5 wt pct Cr-1.5 wt pct Al (*i.e.*, Fe-1.58 at. pct Cr-3.07 at. pct Al) foil. The N content is related to 100 (Fe + Cr + Al) matrix atoms. The $[N]_{(Cr,Al)N}$ is the amount of N required for the precipitation of all Al and Cr as $Cr_{1-x}Al_xN$; $[N]^0_{\alpha\text{-Fe}}$ is the amount of N dissolved in an unstrained pure ferrite matrix at the prenitriding conditions. (*b*) Nitrogen-absorption isotherm of the pre- and denitrided Fe-1.5 wt pct Cr-1.5 wt pct Al foil determined at 833 K for different nitriding potentials (N content related to 100 atoms of Fe + Cr + Al). The N level after denitriding has been indicated by A. The calculated N level $[N]_{(Cr,Al)N}$ has been indicated by C. The linear portion of the absorption isotherm has been indicated by the dashed line that intersects the ordinate at $r_N = 0$ at N level indicated by B. The $[N]_{interface}$, $[N]^0_{\alpha\text{-Fe}}$, and $[N]_{strain}$ denote N adsorbed at the precipitate/matrix interface, N dissolved in unstrained ferrite, and excess nitrogen dissolved in the ferrite matrix due to the precipitate-matrix misfit strain, respectively.

earlier analyses of nitrogen-absorption isotherms recorded for Fe-1 wt pct Cr (*i.e.*, Fe-1.04 at. pct Cr)[52] and Fe-2 wt pct V (*i.e.*, Fe-2.23 at. pct V),[48] such N is conceived as adsorbed at the faces of the tiny, (semi)coherent nitride platelets. The amount of this nitrogen is indicated by $[N]_{interface}$.

Table III. Total N Uptake in Prenitrided (at 853 K) and Denitrided (at 743 K) Fe-1.5 Wt Pct Cr-1.5 Wt Pct Al Foil (*i.e.*, Fe-1.58 At. Pct Cr-3.07 At. Pct Al) Nitrided at 833 K at Different Nitriding Potentials; Values for N Uptake in Unstrained Pure Ferrite (*i.e.*, $[N]^0_{\alpha\text{-Fe}}$) at 833 K for Applied Nitriding Potentials Were Calculated Using Data in References 47 and 52

r_N (atm$^{-1/2}$)	$[N]^{total}$ (at. pct)	$[N]^{total}$ (N at./100 at. Fe + Cr + Al)	$[N]^0_{\alpha\text{-Fe}}$ at 833 K (at. pct)
0	5.20*	5.49*	0
0.054	5.351 ± 0.008	5.654 ± 0.009	0.12
0.091	5.454 ± 0.002	5.769 ± 0.003	0.21
0.117	5.533 ± 0.001	5.857 ± 0.002	0.27
0.140	5.590 ± 0.001	5.921 ± 0.002	0.32

*Estimate: extrapolation of the straight line fitted through the data points to $r_N = 0$ yields the N level B = 5.49 N atoms per 100 atoms of Fe + Cr + Al in Fig. 8(b).

The equilibrium solubility of N in pure, unstrained ferrite $[N]^0_{\alpha\text{-Fe}}$ at temperatures in the range of 773 to 843 K has been determined as a function of the nitriding potential in References 48 and 53. On this basis, the equilibrium solubilities of N in ferrite at 833 K for the different nitriding potentials used in this work have been given in Table III and Figure 8(b).

The subdivision of the total N uptake $[N]_{total}$ in $[N]_{(Cr,Al)N}$, $[N]_{interface}$, $[N]^0_{\alpha\text{-Fe}}$, and $[N]_{strain}$ at the different nitriding potentials has thus been indicated in Figure 8(b). The number of N atoms per 100 atoms of Fe + Cr + Al incorporated in the nitrides (*i.e.*, $[N]_{(Cr,Al)N}$) and adsorbed at the nitride/matrix interface (*i.e.*, $[N]_{interface}$) is obviously independent of the nitriding potential.

The composition of a $Cr_{1-x}Al_xN$ precipitate with adsorbed excess nitrogen $[N]_{interface}$ can be described as $Cr_{1-x}Al_xN_y$, where

$$y = \frac{[N]_{(Cr,Al)N} + [N]_{interface}}{[N]_{(Cr,Al)N}} = \frac{\text{Level B}}{\text{Level C}} = 1.178 \qquad [1]$$

Assuming that all Al and Cr formed cubic $Cr_{1-x}Al_xN_y$ platelets, the value y (Eq. [1]) provides indirect information about the average thickness of a precipitate platelet. As shown in this work, $Cr_{1-x}Al_xN$ precipitates develop as platelets in the cubic, rock-salt structure type obeying a Bain OR with the ferrite matrix. With $\{001\}_{Cr_{1-x}Al_xN}$ as the habit planes (Figure 3), the thickness of a monolayer of $Cr_{1-x}Al_xN$ is one-half of the lattice parameter of the rock-salt structure type (*i.e.*, $\frac{a_{Cr_{1-x}Al_xN}}{2}$). If at every octahedral interstice in the ferrite matrix at the nitride/matrix interface one excess nitrogen atom is trapped, it follows that

$$y = \frac{n+2}{n} \qquad [2]$$

where n is the number of $Cr_{1-x}Al_xN$ monolayers. Hence, the thickness t of a $Cr_{1-x}Al_xN$ platelet follows from

$$t = n \cdot \frac{a_{Cr_{1-x}Al_xN}}{2} = \frac{a_{Cr_{1-x}Al_xN}}{y-1} \quad [3]$$

With $a_{Cr_{1-x}Al_xN} \approx 0.411$ nm,[53] the estimated average thickness t of a precipitate in the nitrided (at 853 K) foil is 2.3 nm.

IV. GENERAL DISCUSSION

A. *Combined Precipitation of Al and Cr in Mixed-nitride Precipitates*

The equilibrium nitride precipitates developing in Fe-Cr and Fe-Al alloys are of a cubic, rock-salt structure type CrN[6,11,15–21] and hexagonal, wurtzite structure type AlN.[5,22–28] The results obtained in this work show unambiguously that nitride precipitates developing in Fe-Cr-Al alloys are of the mixed type: cubic, rock-salt structure type $Cr_{1-x}Al_xN$ precipitates (Sections III–C–1 through 3). This finding can be interpreted as a metastable, intermediate stage of nitride precipitation in this system: Indeed, annealing of the nitrided system at an elevated temperature (168 hours at 973 K) caused replacement of the mixed cubic, rock-salt structure type $Cr_{1-x}Al_xN$ precipitates by the equilibrium cubic, rock-salt structure type CrN and equilibrium hexagonal, wurtzite structure type AlN, involving a separation of the alloying elements (XRD, TEM, and STEM analyses presented and discussed in Reference 55).

At the nitriding temperature, the diffusion of the alloying elements Cr and Al is relatively slow enough[§§] that the Al atoms are "dragged" into the developing cubic, rock-salt structure type CrN precipitates: There is no time to diffuse away and form hexagonal, wurtzite structure type AlN precipitates (a process that is slow, in any case, due to the relatively large amount of misfit energy to be accommodated[26]). In other words, the system accepts the gain of a smaller-than-maximal amount of energy, released by nitride precipitation, as an intermediate solution: the development of mixed, cubic, rock-salt structure type $Cr_{1-x}Al_xN$ precipitates. The presence of Cr assures that substantial energy is set free upon precipitation of this mixed nitride, whereas this would not hold for precipitation of a cubic, rock-salt structure type AlN (Reference 26). Further, the development of the cubic, rock-salt structure type mixed $Cr_{1-x}Al_xN$ precipitates is facilitated by nearly the same values for the lattice parameters of cubic, rock-salt structure type CrN and AlN: The sizes of the Cr and Al atoms/ions in this structure are nearly the same.

[§§]For 1 hour at 853 K, $\sqrt{Dt}$ (with D = diffusion coefficient of Me in ferrite and t = diffusion (*i.e.*, nitriding) time) equals 19 nm for Cr and 13 nm for Al using diffusion data from Refs. 56 and 57, whereas $\sqrt{Dt}$ for nitrogen in pure ferrite equals $2{\cdot}10^5$ nm, using diffusion data from Ref. 58.

B. *Precipitate Morphology and Coherency Effects*

The mixed $Cr_{1-x}Al_xN$ precipitates exhibit a platelike morphology, with the platelets following a Bain-type OR with the ferrite matrix, with $\{001\}_{\alpha\text{-Fe}}$ planes parallel to the platelet faces. The platelet morphology is a consequence of the strongly anisotropic nature of the misfit with the surrounding matrix: The linear misfits along and perpendicular to the $\{001\}_{\alpha\text{-Fe}}$ habit planes are maximally approximately 0.02 and 0.44, respectively, as estimated from the data for pure CrN and AlN (cubic, rock-salt structure type).[25,36]

Especially if the platelet precipitates become larger and thicker (per the observations at larger depths beneath the surface in Section C), the platelets become partly nonplanar and distorted (with curvature and contrast variation along the platelets and the spreading of $\{002\}_{Cr_{1-x}Al_xN}$ diffraction spots, per Figures 4(a) and (5)). This observation may be related to the results reported in Reference 16, in which for thin platelets of TiN and CrN in ferrite the Bain OR and for coarser precipitates the Nishiyama–Wassermann OR was observed. Indeed, a rotation of only 9.74 deg around $[001]_{\alpha\text{-Fe}}$ suffices to convert a Bain OR into a Nishiyama–Wassermann OR.[60,61] For the case of fcc precipitates in a bcc matrix, it may generally be expected that a continuous distribution of ORs deviating a few degrees by rotation around some axis from the Bain OR can occur, depending on the precise state of local misfit.[54,59,62–65]

The absence of separate nitride diffraction peaks in the X-ray diffractogram is associated with the largely coherent nature of the precipitate/matrix system: The surrounding ferrite matrix is distorted tetragonally, due to the misfit between the nitride platelets and the ferrite lattice. The system composed of a coherent platelet and its tetragonally distorted ferrite surroundings diffracts coherently, giving rise to strongly broadened asymmetrical ferrite reflections (Figure 1), as has recently been discussed for VN platelets in ferrite.[59] The occurrence of many finely distributed, tiny, coherent precipitates in the ferrite matrix explains the very high hardness values observed near the surface of approximately 1200 HV (for a load of 0.015 kg) (Figure 2(c)), as compared to the hardness in the unnitrided core, which is approximately 150 HV (for a load of 0.015 kg).

C. *Depth Gradient of Precipitate Size*

The length of the precipitates near the surface is approximately 10 nm (and smaller); their thickness is approximately 1 nm (Figures 3(a) and (b) and 6(b)). Deeper in the nitrided layer (at depths of approximately 140 and 215 μm), the precipitates are coarser than they are nearer the surface: The length of the precipitates here is approximately 100 nm, whereas their thickness is in the range of approximately 5 to 10 nm (Figures 4(a) and 5(a)).

The nitrogen supersaturation is higher nearer the surface than in deeper regions within the nitrided zone (this is a consequence of the need to maintain a nitrogen flux throughout the nitrided zone during nitriding). Hence, the driving force for nitride precipitation is

higher nearer the surface than at larger depths. Consequently, a higher nitride-nucleus density can occur near the surface. This is compatible with the observation of more and finer nitride precipitates nearer the surface (Figures 3(a) and (b)) than at larger depths (Figures 4 and 5).[¶]

[¶]A related phenomenon has been discussed on the same basis: the occurrence of a larger number of α-Fe/CrN lamellar colonies of smaller lamellar spacing nearer the surface of nitrided Fe-Cr alloys than at larger depths.[21]

D. *Excess Nitrogen*

The presence of excess nitrogen is a consequence of the coherency at the precipitate/matrix interface: The elastic accommodation of the misfit induces an elastic strain field in the matrix that allows the dissolution of mobile extra nitrogen in the ferrite matrix; at octahedral interstices in the ferrite matrix adjacent to the platelet faces, nitrogen atoms, *via* bonding to Cr or Al in the platelet, can be adsorbed, *i.e.*, (immobile) excess nitrogen.[36] Evidently, the coherency can be more pronounced the smaller and thinner the platelet. Hence, the occurrence of more excess nitrogen in the near-surface region (Figure 2(b) and its caption and Figure 6) can be a straightforward consequence of the platelets being smaller and thinner in the near-surface region than at larger depths (Section C).

After denitriding 0.08 at. pct, excess nitrogen remains in the foil (Figure 8(b); difference of levels A and C). This remaining excess nitrogen is apparently strongly bonded at the precipitate/matrix interface and cannot be removed easily, even after longer denitriding times. This behavior is only known from nitrided Fe-Al alloys.[24,49] Thus, it may be suggested that, in particular, the aluminum in the $Cr_{1-x}Al_xN$ precipitates has a strong affinity for nitrogen and the adsorbed excess nitrogen remaining after denitriding is the adsorbed excess nitrogen that is bonded to Al in the $Cr_{1-x}Al_xN$ platelet.

V. CONCLUSIONS

The following conclusions are drawn from this study.

1. The nitriding of ternary iron-based Fe-Cr-Al alloys leads to the precipitation of cubic, rock-salt crystal structure type, mixed $Cr_{1-x}Al_xN$ precipitates. These precipitates do not represent thermodynamic equilibrium, which would involve precipitation of cubic, rock-salt structure type CrN and hexagonal, wurtzite structure type AlN. The cubic, rock-salt structure type mixed $Cr_{1-x}Al_xN$ precipitates develop because the diffusion of Cr and Al in ferrite, as compared to diffusion of N in ferrite, is very slow and the precipitation of hexagonal, wurtzite structure type AlN is a process with difficult nucleation.
2. The $Cr_{1-x}Al_xN$ precipitates develop as platelets initially partially coherent with the ferrite matrix according to the Bain OR. At the initial stage of nitride formation, the nitride platelets diffract coherently with the matrix; separate nitride reflections do not occur in the X-ray diffractogram.
3. More and finer nitride precipitates occur nearer the surface than at larger depths beneath the surface, because the driving force for nitride precipitation is largest near the surface.
4. For coarser nitride platelets (*i.e.*, at larger depths, as discussed earlier), the precipitates are partly nonplanar/distorted (curvature and contrast variation along the platelets in transmission electron micrographs and spreading (splitting up) of electron diffraction spots).
5. Large amounts of excess nitrogen, 1.26 at. pct in excess of the "normal" uptake of 4.65 at. pct, are taken up upon precipitation of the $Cr_{1-x}Al_xN$ precipitates, as a result of the elastic accommodation of the precipitate/matrix misfit. The excess nitrogen uptake is largest near the surface, because the finest precipitates occur there (as discussed earlier) and are subjected to (almost) full elastic accommodation of the precipitate/matrix misfit.
6. The excess nitrogen remaining after denitriding is ascribed to those nitrogen atoms that are strongly bonded at the platelet surfaces to, in particular, the Al atoms in the mixed nitride at the platelet surfaces.

ACKNOWLEDGMENTS

The authors thank Messrs. J. Köhler and P. Kress for assistance with the nitriding experiments, Mrs. S. Haug for assistance with the EPMA experiments, Mr. W.-D. Lang for TEM sample preparation, Mrs. M. Kelsch for assistance during the first stage of the TEM experiments, Dr. F. Phillipp for assistance during the first stage of the HRTEM experiments, Dr. W. Sigle for assistance during the STEM experiments and for discussion and critical reading of the manuscript, and Dr. A. Leineweber for discussion.

OPEN ACCESS

REFERENCES

1. C.H. Knerr, T.C. Rose, and J.H. Filkowski: in *ASM Handbook: Heat Treating*, J.R. Davis, G.M. Davidson, S.R. Lampman, T.B. Zorc, J.L. Daquila, A.W. Ronke, K.L. Henniger, and R.C. Uhl, eds., ASM INTERNATIONAL, Metals Park, OH, 1991, vol. 4, p. 387.
2. E.J. Mittemeijer: *Proc. AWT-Tagung Nitrieren und Nitrocarburieren*, E.J. Mittemeijer and J. Grosch, eds., Arbeitsgemeinschaft Wärmebehandlung und Werkstofftechnik e.V., Wiesbaden, Germany, 1991.

3. D. Liedtke, U. Baudis, J. Boßlet, U. Huchel, H. Klümper-Westkamp, W. Lerche, and H.J. Spies: *Wärmebehandlung von Eisenwerkstoffen Nitrieren und Nitrocarburieren*, Expert Verlag, Renningen, 2006.
4. E.J. Mittemeijer and J.T. Slycke: *Surf. Eng.*, 1996, vol. 12, p. 152.
5. M.H. Biglari, C.M. Brakman, and E.J. Mittemeijer: *Philos. Mag. A*, 1995, vol. 72, p. 1281.
6. R.E. Schacherl, P.C.J. Graat, and E.J. Mittemeijer: *Z. Metallkd.*, 2002, vol. 93, p. 468.
7. D.H. Jack: *Acta Metall.*, 1976, vol. 24, p. 137.
8. S.S. Hosmani, R.E. Schacherl, and E.J. Mittemeijer: *Acta Mater.*, 2005, vol. 53, p. 2069.
9. E.C. Bain: *Trans. AIME*, 1924, vol. 70, p. 25.
10. R.G. Baker and J. Nutting: *Iron Steel Inst. Spec. Rep.*, 1959, vol. 64, p. 1.
11. B. Mortimer, P. Grieveson, and K.H. Jack: *Scand. J. Metall.*, 1972, vol. 1, p. 203.
12. M. Pope, P. Grieveson, and K.H. Jack: *Scand. J. Metall.*, 1973, vol. 2, p. 29.
13. J.H. Driver, D.C. Unthank, and K.H. Jack: *Philos. Mag.*, 1972, vol. 26, p. 1227.
14. B.J. Lightfoot and D.H. Jack: *Proc. Conf. Heat Treatment*, London, 1973, TMS, Warrendale, PA, 1975, p. 59.
15. P.M. Hekker, H.C.F. Rozendaal, and E.J. Mittemeijer: *J. Mater. Sci.*, 1985, vol. 20, p. 718.
16. N.G. Chechenin, P.M. Bronsveld, A. Chezan, C.B. Craus, D.O. Boerma, J.T.M. De Hosson, and L. Niesen: *Phys. Status Solidi A*, 2000, vol. 177, p. 117.
17. M. Sennour, P.H. Jouneau, and C.J. Esnouf: *J. Mater. Sci.*, 2004, vol. 39, p. 4521.
18. R.E. Schacherl, P. Zieba, and E.J. Mittemeijer: *Defect. Diffusion Forum*, 2005, vols. 237–240, p. 1270.
19. S.S. Hosmani, R.E. Schacherl, and E.J. Mittemeijer: *Mater. Sci. Technol.*, 2005, vol. 21, p. 113.
20. S.S. Hosmani, R.E. Schacherl, and E.J. Mittemeijer: *Int. J. Mater. Res.*, 2006, vol. 97, p. 1545.
21. N.E. Vives Diaz, R.E. Schacherl, and E.J. Mittemeijer: *Int. J. Mater. Res.*, 2008, vol. 99, p. 150.
22. K. Bohnenkamp: *Arch. Eisenhüttenwes.*, 1967, vol. 38, p. 433.
23. H.H. Podgurski and H.E. Knechtel: *Trans. TMS-AIME*, 1969, vol. 245, p. 1595.
24. H.H. Podgurski, R.A. Oriani, F.N. Davis, J.C.M. Li, and Y.T. Chou: *Trans. TMS-AIME*, 1969, vol. 245, p. 1603.
25. M.H. Biglari, C.M. Brakman, M.A.J. Somers, W.G. Sloof, and E.J. Mittemeijer: *Z. Metallkd.*, 1993, vol. 84, p. 124.
26. M.H. Biglari, C.M. Brakman, E.J. Mittemeijer, and S. van der Zwaag: *Metall. Mater. Trans. A*, 1995, vol. 26, p. 765.
27. H.J. Spies, H. Biermann, and A. Fischer: *Z. Metallkd.*, 2005, vol. 96, p. 781.
28. S. Meka, S.S. Hosmani, A.R. Clauss, and E.J. Mittemeijer: *Int. J. Mater. Res.*, 2008, vol. 99, p. 808.
29. H.H. Landolt and R.B. Börnstein: *Numerical Data and Functional Relationships in Science and Technology, New Series, Group III: Crystal and Solid State Physics*, Springer-Verlag, Berlin, 1978, vol. 7c.
30. Q. Xia, H. Xia, and A.L. Ruoff: *J. Appl. Phys.*, 1993, vol. 73, p. 8198.
31. W. Mader, D. Birkhölzer, and H. Ichinose: *DVS-Berichte*, 1990, vol. 129, p. 93.
32. I. Petrov, E. Mojab, R.C. Powell, J.E. Greene, L. Hultman, and J.E. Sundgren: *Appl. Phys. Lett.*, 1992, vol. 60, p. 2491.
33. K.H. Jack: *Proc. Conf. Heat Treatment*, London, TMS, Warrendale, PA, 1975, p. 39.
34. J.S. Steenaert, M.H. Biglari, C.M. Brakman, E.J. Mittemeijer, and S. van der Zwaag: *Z. Metallkd.*, 1995, vol. 86, p. 700.
35. W. Pitsch and A. Schrader: *Arch. Eisenhüttenwes.*, 1958, vol. 29, p. 715.
36. M.A.J. Somers, R.M. Lankreijer, and E.J. Mittemeijer: *Philos. Mag. A*, 1989, vol. 59, p. 353.
37. V.A. Phillips and A.U. Seybolt: *Trans. TMS-AIME*, 1968, vol. 242, p. 2415.
38. W. Koch, C. Ilschner-Gensch, and H. Rohde: *Arch. Eisenhüttenwes.*, 1956, vol. 27, p. 701.
39. L. Rademacher, M. Hoock, and K.K. Mehta: *Thyssen Edelst. Techn. Ber.*, 1979, vol. 5, p. 162.
40. R. Wiedemann, H. Oettel, and D. Bergner: *HTM*, 1992, vol. 47, p. 14.
41. V. Massardier, L. Voron, C. Esnouf, and J. Merlin: *J. Mater. Sci.*, 2001, vol. 36, p. 1363.
42. E.J. Mittemeijer and M.A.J. Somers: *Surf. Eng.*, 1997, vol. 13, p. 483.
43. A. Strecker, U. Salzberger, and J. Mayer: *Prakt. Metallogr.*, 1993, vol. 30, p. 482.
44. JCPDS-International Centre for Diffraction Data, Newtown Square, PA, 2002.
45. J.L. Pouchou and F. Pichoir: *Rech. Aerosp.*, 1984, p.167.
46. A. Barna: *Specimen Preparation for Transmission Electron Microscopy of Materials—III*, Materials Research Society, Warrendale, PA, 1992, vol. 254, p. 3.
47. D.B. Williams and C.B. Carter: *Transmission Electron Microscopy*, Plenum Press, New York, NY, 1996.
48. S.S. Hosmani, R.E. Schacherl, and E.J. Mittemeijer: *Acta Mater.*, 2006, vol. 54, p. 2783.
49. M.H. Biglari, C.M. Brakman, E.J. Mittemeijer, and S. van der Zwaag: *Philos. Mag. A*, 1995, vol. 72, p. 931.
50. S. Chen and J. Morris: *Metall. Mater. Trans. A*, 1977, vol. 8, p. 19.
51. G. Cliff and G.W. Lorimer: *J. Microsc-Oxf.*, 1975, vol. 103, p. 203.
52. S.S. Hosmani, R.E. Schacherl, and E.J. Mittemeijer: *J. Mater. Sci.*, 2008, vol. 43, p. 2618.
53. S.S. Hosmani, R.E. Schacherl, L. Litynska-Dobrzynska, and E.J. Mittemeijer: *Philos. Mag.*, 2009, vol. 89, p. 565.
54. P.H. Mayrhofer, D. Music, T. Reeswinkel, H.G. Fuss, and J.M. Schneider: *Acta Mater.*, 2008, vol. 56, p. 2469.
55. A.R. Clauss, E. Bischoff, R.E. Schacherl, and E.J. Mittemeijer: unpublished research.
56. C.G. Lee, Y. Iijima, T. Hiratani, and K. Hirano: *Mater. Trans.*, 1990, vol. 31, p. 255.
57. M. Gemmaz, M. Afyouni, and A. Mosser: *Surf. Sci.*, 1990, vol. 227, p. L109.
58. J.D. Fast and M.B. Verrijp: *J. Iron Steel Inst.*, 1954, vol. 176, p. 24.
59. N.E. Vives Diaz, S.S. Hosmani, R.E. Schacherl, and E.J. Mittemeijer: *Acta Mater.*, 2008, vol. 56, p. 4137.
60. Z. Nishiyama: *Sci. Rep. Tohoku Univ.*, 1934, vol. 23, p. 637.
61. G. Wassermann: *Arch. Eisenhüttenwes.*, 1933, vol. 6, p. 347.
62. U. Dahmen: *Acta Metall.*, 1982, vol. 30, p. 63.
63. Y.L. He, S. Godet, and J.J. Jonas: *J. Appl. Cryst.*, 2006, vol. 39, p. 72.
64. J.F. Nie: *Acta Mater.*, 2008, vol. 56, p. 3169.
65. P.M. Kelly and M.X. Zhang: *Mater. Forum*, 1999, vol. 23, p. 41.
66. A.R. Clauss, R.E. Schacherl, and E.J. Mittemeijer: unpublished research.